Available online at www.sciencedirect.com

SciVerse ScienceDirect

Ceramics International 39 (2013) 5459–5465

CERAMICS INTERNATIONAL

www.elsevier.com/locate/ceramint

Assessment of redox behavior of nickel ferrite as oxygen carriers for chemical looping process

Yu-Lin Kuo[a,*], Weu-Mau Hsu[a], Ping-Chin Chiu[b], Yao-Hsuan Tseng[b], Young Ku[b]

[a]Department of Mechanical Engineering, National Taiwan University of Science and Technology, Taipei 10607, Taiwan
[b]Department of Chemical Engineering, National Taiwan University of Science and Technology, Taipei 10607, Taiwan

Received 17 September 2012; received in revised form 27 November 2012; accepted 14 December 2012
Available online 26 December 2012

Abstract

This study investigated the suitability of using nickel ferrite ($NiFe_2O_4$) oxygen carriers for a chemical looping process. $NiFe_2O_4$ powder was prepared by ball milling equimolar NiO and Fe_2O_3 in a high temperature solid-state reaction. Material characteristics of $NiFe_2O_4$ samples were investigated by X-ray diffraction (XRD), Brunauer–Emmett–Teller (BET) surface area measurements, and scanning electron microscopy (SEM). Redox cycling of $NiFe_2O_4$ oxygen carriers was performed by thermogravimetric (TGA) measurement under pure CH_4 gas and O_2/Air atmospheres, respectively. After five successive cycles, $NiFe_2O_4$ powder with a single phase of spinel structure demonstrated higher redox cycling behavior and better stability than standard NiO and Fe_2O_3. We also addressed the mechanism underlying the redox cycling by $NiFe_2O_4$ spinel powder. Our results demonstrate the feasibility of using the proposed preparation of $NiFe_2O_4$ as an oxygen carrier in a reversible chemical looping process (CLP).
© 2013 Elsevier Ltd and Techna Group S.r.l. All rights reserved.

Keywords: Nickel ferrite; Redox cycling; Oxygen carriers; Chemical looping process

1. Introduction

Carbon dioxide (CO_2) generated by the combustion of fossil fuels is the greenhouse gas primarily responsible for global warming [1]. The chemical looping process (CLP) has been proposed as a cost effective scheme for separating CO_2 from the emissions produced by burning coal [2–5]. Lewis and Gilliland patented the production of pure carbon dioxide using metal oxides as a means to process the cyclic reduction and oxidation (redox) reactions in two interconnected fluidized beds [6]. CLP involves the use of metal oxides as carriers to transport lattice oxygen to react directly with fuels during reduction, thereby avoiding direct contact between fuel and air. During oxidation, the reduced metal oxide is re-oxidized to its original form by combustion in air. The primary benefit of CLP technology is the production of pure CO_2 and stream (H_2O) without the need to expend energy in the separation of CO_2 and N_2. In addition, the CLP process associated with cyclic redox reactions is exothermic [7].

Selection of the oxygen carrier is a key step in the development of CLP technology to ensure continuous reaction in the fuel reactor and air reactor. Previous researches into the thermodynamic properties, reactivity, recyclability, and mechanical strength of oxygen carriers have indicated the applicability of Fe, Ni, Cu, Mn, and Co oxides as candidates in CLP technology [5–10]. Fan et al. [5,11] compared key properties of various metal oxide candidates, determining that iron-based oxygen carriers possess higher oxygen carrying capacity, a higher melting temperature, and suitable mechanical strength, making them a favorable choice for CLP. However, the less poor reactivity of α-Fe_2O_3 with fuels is considered a complicated gas–solid reaction due to the several structural changes involved [12–14]. Nonetheless, the appropriate doping of metal oxides to form composites is viewed as a promising approach to increasing reactivity [15–18].

Shimokawabe et al. [14] reported the applicability of 13 metal oxides as doping agents to alter the reactivity of α-Fe_2O_3. The results of TGA testing on the hydrogen

*Correspondence to: No.43, Section 4, Keelung Road, Taipei 10607, Taiwan. Tel.: +886 2 27376784; fax: +886 2 27376460.
E-mail address: ylkuo@mail.ntust.edu.tw (Y.-L. Kuo).

0272-8842/$ - see front matter © 2013 Elsevier Ltd and Techna Group S.r.l. All rights reserved.
http://dx.doi.org/10.1016/j.ceramint.2012.12.055

reduction of α-Fe_2O_3 demonstrated how the preparation of the oxide influences reactivity. All of these doping agents, except TiO_2, lowered the reduction temperature of α-Fe_2O_3, demonstrating that the addition of metal oxides, such as CuO and NiO, could improve the reactivity of α-Fe_2O_3 under reducing species (H_2 or CH_4 gases). These findings were supported by those of Peňa et al. [19].

In our on-going study on the preparation of NiO–Fe_2O_3 composites as oxygen carriers in CLP, the composite demonstrated superior redox cycling behavior under CH_4 atmosphere in a TGA system. Meanwhile, spinel $NiFe_2O_4$ phase was observed in NiO–Fe_2O_3 composites after the redox cycling test. Therefore, the objective of this study was to evaluate the redox cycling of spinel $NiFe_2O_4$ as an oxygen carrier. XRD and SEM were used to examine the crystal structure and microstructural morphology of the prepared powder. The reduction kinetics of $NiFe_2O_4$ powder at temperatures of 600–1000 °C under a reducing atmosphere was performed using TGA. An additional H_2 evolution profile was performed during the H_2O decomposition with reduced $NiFe_2O_4$ in a fixed bed reactor. The mechanism underlying redox cycling by spinel $NiFe_2O_4$ powder is also discussed in this paper.

2. Experimental details

2.1. Powder preparation and the characterization of materials

Nickel ferrite ($NiFe_2O_4$) was prepared using the conventional ceramic method from an equimolar mixture of NiO and Fe_2O_3. The initial materials used were high purity NiO (99.9%, Aldrich) with a particle size of 20 μm, and high purity α-Fe_2O_3 (99.9%, China Steel) with a particle size of 90 μm. For the preparation of $NiFe_2O_4$, the raw materials were physically mixed and ground for 2 h in ethyl alcohol using high energy ball milling in a planetary ball mill (Model PM100, Retsch, GmbH, Germany). Zirconium oxide grinding jars (volume 50 mL) containing balls and a mixture of powders were arranged on the sun wheel of the planetary ball mill in the direction opposite to the movement of the sun wheel with a rotation speed ratio of 1:−2. The rotation speed of the sun wheel was maintained at 380 rpm. The mass ratios of the zirconium balls (1 mm in diameter) ball-to-material and solvent-to-material were fixed at 5:1 and 2:3, respectively. The obtained slurry was dried in a vacuum evaporator at 60 °C, whereupon the dry powder was calcined at a heating rate of 10 °C/min using a programmable cube furnace in air at 1200 °C for 2 h to form the ferrite phase.

$$NiO + Fe_2O_3 \rightarrow NiFe_2O_4 \quad (1)$$

The exact spinel ferrite phase of the material was examined using X-ray diffraction (Bruker D2 Phaser, Cu-Kα radiation with $\lambda = 1.5405$ Å), at a scanning rate of $0.05^\circ/s^{-1}$ in the 2θ range, between 20° and 80°. Field emission scanning electron microscopy (FESEM, JOEL JSM-6500 F) was used to observe the microstructural morphology and grain size of the samples.

2.2. Tests of redox cycling and H_2 production by water-splitting

A Netzsch STA 449F3 thermogravimetric analyzer (TGA) was used to analyze the redox cycling of the prepared $NiFe_2O_4$ oxygen carriers. Three inlet flows provided reducing gas (20% CH_4), oxidizing gas (air), and purging gas (N_2). Programmable switching was used to control the inlet flow using mass flow controllers (Fujikin T1000) to perform redox cycles of $NiFe_2O_4$ oxygen carriers. Initially, 200 mg of powder samples was placed in an alumina crucible in air, and heated to the desired temperatures at a ramping rate of 10 °C/min under N_2 atmosphere. The first reduction was then performed using 200 mL/min of 20% CH_4, followed by a purge with 200 mL/min of N_2, oxidization with 200 mL/min of air, and final purging with 200 mL/min of N_2.

To evaluate the ability of prepared $NiFe_2O_4$ to generate H_2, we employed a fixed bed reactor (FBR) comprising a 316 stainless steel reactor with an inner diameter of 2.54 cm, and a bed height of 20 cm in the heating section. A 16-aperture supporting plate was fixed within the reactor to facilitate the loading of oxygen carrier pellets (each aperture was 0.25 mm in diameter). The heating element was equipped with a thermocouple to measure the actual temperature within the reactor and was controlled by a proportional integral derivative controller. The FBR was loaded with 1.0 g of prepared $NiFe_2O_4$ pellets. The temperature of FBR was increased using a muffle furnace from room temperature to 900 °C in N_2 atmosphere. Reducing gas comprising 20% CH_4 balanced by N_2 was injected into the FBR at a rate of 300 mL/min for 40 min. N_2 gas was used to purge the FBR of residual reducing gas prior to the water-splitting process. To test for the production of H_2 by water-splitting, steam was generated at an injection rate of 300 mL/min controlled using a syringe pump (KD Scientific KDS100). Surplus steam was cooled and collected using a cold trap device. A gas chromatographic (GC) analyzer equipped with thermal conductivity detector (Agilent 7890) was used to measure the concentration of H_2 gas.

3. Results and discussions

We first examined the spinel $NiFe_2O_4$ using XRD. Fig. 1 shows the evolution in XRD patterns for the mixtures of NiO + Fe_2O_3 before and after calcination in air at 1200 °C. As shown in Fig. 1(d), the calcined powder revealed a single phase of $NiFe_2O_4$ with a cubic-spinel structure; the strongest diffraction peak of (311) plane was recorded at a 2θ of 35.7°. The calculated lattice parameter of calcined $NiFe_2O_4$ ($a = 8.332$ Å) was in a good agreement with previous studies and the corresponding Joint Commission

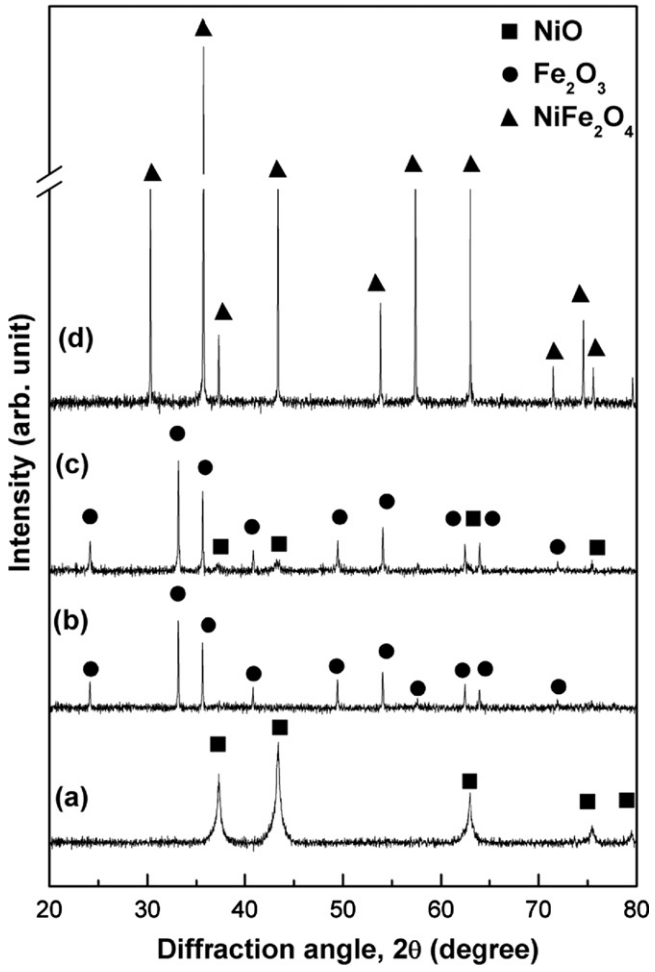

Fig. 1. X-ray diffraction patterns: (a) NiO, (b) Fe_2O_3, (c) physically mixed NiO + Fe_2O_3 before calcination; and (d) following calcination in air at 1200 °C.

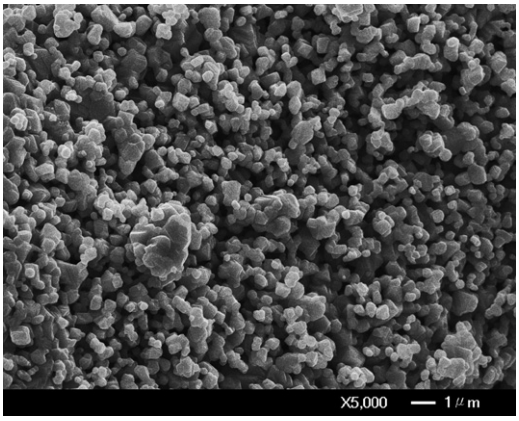

Fig. 2. SEM micrographs of prepared $NiFe_2O_4$ powder.

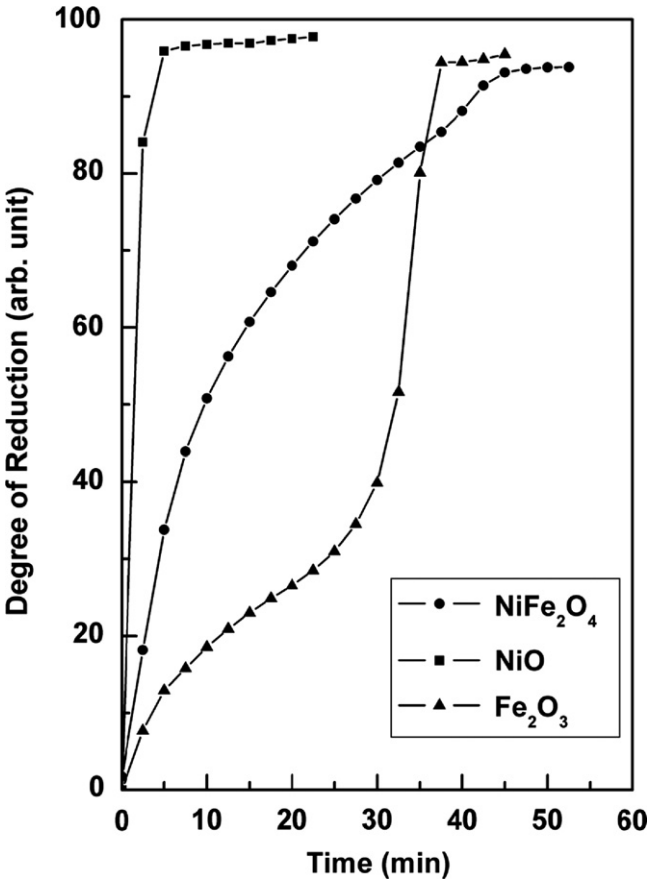

Fig. 3. Degree of reduction for NiO, Fe_2O_3 and $NiFe_2O_4$ under 20 vol% CH_4 atmosphere.

on Powder Diffraction Standards (JCPDs) file card (054-0964) [19,20]. From the XRD results, we also determined the crystal size of $NiFe_2O_4$ from the broadening in the diffraction peak, employing the Scherrer formula as expressed by:

$$t = \frac{0.9\lambda}{B\cos\theta} \quad (2)$$

where t is the crystal size, λ is the X-ray wavelength corresponding to Cu K_α radiation, θ is the diffraction angle, and B is the full width half maximum (FWHM) of the diffraction (311) peak. The size of crystals was also calculated for (220) and (440) planes with an average value of approximately 200 nm. However, the particles of prepared $NiFe_2O_4$ powder with well-defined crystalline structures were homogeneously distributed in the size range of 200–500 nm shown in Fig. 2.

In Fig. 3, the isothermal reduction of NiO, Fe_2O_3, and $NiFe_2O_4$ were conducted in a TGA system at 900 °C using 20 vol% methane (CH_4) as a reducing gas. The degree of reduction (DOR) of the powder was defined as the ratio of weight loss at a fixed time to the total weight loss after the complete reduction (the theoretical maximum oxygen capacity) [19]. The theoretical maximum oxygen capacity for NiO, Fe_2O_3 and $NiFe_2O_4$ are 21 wt%, 30 wt% and 27.2 wt%, respectively.

According to the Bell's diagram, the kinetics of a reduction of hematite (Fe_2O_3) under reducing species is considered a complex gas–solid reaction, due to several structural changes via magnetite (Fe_3O_4), wüstite ($Fe_{1-x}O$) and metal iron (Fe) [12,13]. Pineau at al. [21] found that

the reduction path of magnetite to iron is related mainly to reduction temperature. Above 570 °C, magnetite can be fully reduced to wüstite prior to its reduction to metal iron. The reduction path of Fe_2O_3 provides several pathways to obtain metal iron, described as follows [12,13,19–21]:

$$Reduction\ over\ 570^{\circ}C: Fe_2O_3 \rightarrow Fe_3O_4 \rightarrow Fe_{1-x}O \rightarrow Fe \quad (3)$$

A typical reduction curve of Fe_2O_3 represents three transitions of intermediate oxides under CH_4 atmosphere, as shown in Fig. 3. The first transition below 20% implies a stepwise reduction of hematite (Fe_2O_3) to magnetite (Fe_3O_4, DOR: 11%), subsequently proceeding to the second transition to wüstite ($Fe_{1-x}O$, DOR: 25%) below 40%. Above 40%, wüstite was further reduced to metal iron. Peña et al. performed XDR analysis on intermediate iron oxides, indicating that a partially (approximately 11%) reduced sample was composed mainly of magnetite (Fe_3O_4), and peaks of metal iron were observed only in completely reduced samples [19]. Based on the results of TGA and XRD, the mechanism underlying the kinetics of reduction for hematite (Fe_2O_3) could be addressed as Eq. (3).

At a reducing temperature of 900 °C, NiO transformed into metallic nickel within 3min, indicating that NiO has relatively high reduction kinetics, compared to hematite (Fe_2O_3). However, NiO has an intrinsically lower oxygen capacity of 21%, lower physical strength, and is hazardous to the environment and human health, making it unsuitable for use as an oxygen carrier for CLP [5,11].

The addition of various metal oxides, such as NiO, CuO_x, LiO, and TiO_2 has been proposed to overcome the low reduction kinetics of hematite (Fe_2O_3). Shimokawabe et al. [14] proved that metal oxides with oxidation number +2 (NiO and CuO) form metal ferrites (MFe_2O_4, M: Ni or Cu) with higher reduction kinetics. As shown in Fig. 3, only one stepwise reduction process was observed in the prepared $NiFe_2O_4$ under CH_4 atmosphere, indicating that the addition of nickel oxide to hematite (Fe_2O_3) could recover the lower reduction kinetics [19].

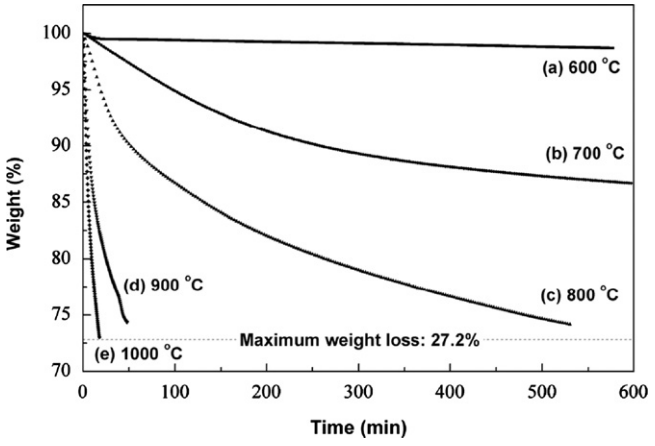

Fig. 4. Reduction isotherms of nickel ferrite versus reaction time under 20 vol% CH_4 atmosphere at various temperatures.

As shown in Fig. 4, the reduction isotherms of nickel ferrite versus the reaction time at various temperatures were monitored according to changes in weight under a 20 vol% methane (CH_4) atmosphere. The change in weight of nickel ferrite indicated inferior reduction behavior at lower temperatures of 600 and 700 °C. The time required for the (nearly) complete reduction of nickel ferrite was approximately 530, 46, and 16 min at temperatures of 800, 900, and 1000 °C, respectively. In addition, none of the oxides under CH_4 atmosphere reached complete reduction due to the formation of a compact metallic layer surrounded the oxide particles. Pineau et al. described how the metallic layer hindered the diffusion of reducing species into the unreacted oxide region within the particles, which subsequently slowed the reduction rate [21].

Furthermore, there was an increase in the initial reduction (up to 10 wt% loss) following an increase in reduction temperature, which might be attributed to a stronger reduction mechanism at higher temperatures. To identify the initial reduction mechanism of $NiFe_2O_4$, we obtained the activation energy (Ea) of the reduction behavior using the reduction rate equation (Eq. 4) and Arrhenius equation (Eq. 5):

$$\frac{dR}{dt} = K_R P^m \quad (4)$$

$$K_R = K_{R0} \exp(-Ea/RT) \quad (5)$$

where dR/dt is the reduction rate, K_R is the reduction rate constant, P is the pressure of the reducing gases, m is the order of reduction, K_{R0} is the frequency factor, R is the gas constant, and T is the absolute temperature. In Fig. 5, we present the initial reduction rates of $NiFe_2O_4$ as a function of reduction temperature (700–100 °C) using the Arrhenius plots. The calculated Ea values obtained from the plots are also shown in Fig. 5. The experimental results indicate that, above 900 °C (Ea: 55.3 kJ/mol), the reduction process was dominated by a combination of gaseous diffusion and interfacial chemical reaction, while below 900 °C (Ea: 169.2 kJ/mol), the reduction process was controlled by solid-state diffusion. The solid-state diffusion referred to by Khedr is the transport of metal from the points where oxygen is removed to points where nucleation and grain growth occur [22–23]. Compared to the reduction behavior of gas diffusion control (Ea: 8–16 kJ/mol) and interfacial chemical diffusion control (Ea: 60–67 kJ/mol), solid-state diffusion control (Ea: > 90 kJ/mol) hinders the reduction kinetics of materials [22–23]. However, at 1000 °C, serious coking was observed due to the metallic nickel layer acting as a catalyst in the decomposition of CH_4 fuel gas, as the sample approached a 27% loss in weight. Thus, the reduction of $NiFe_2O_4$ using CH_4 gas at 900 °C is believed to be the optimal temperature for a practical implementation of the chemical looping process [5,11].

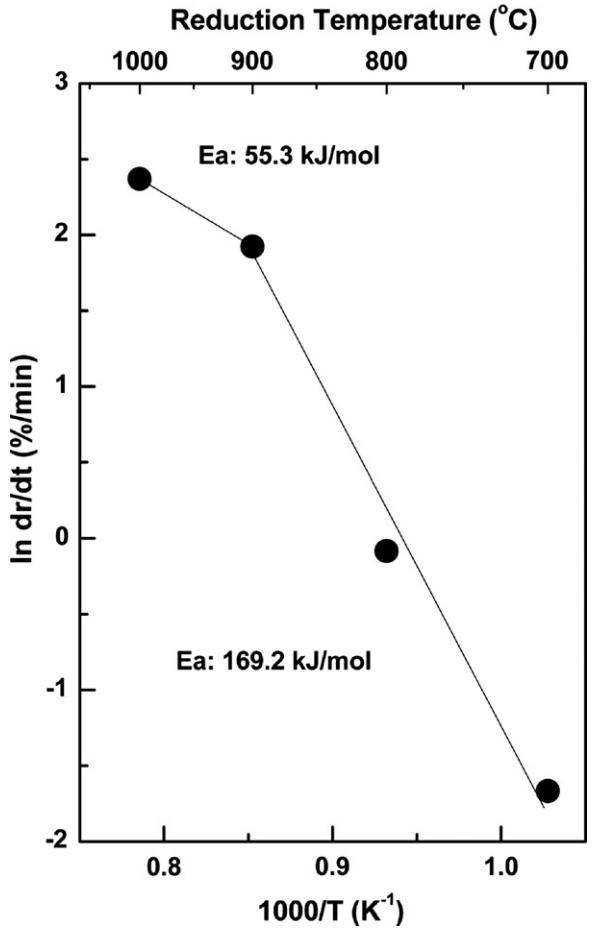

Fig. 5. Arrhenius plots for reduction of $NiFe_2O_4$ in initial stage.

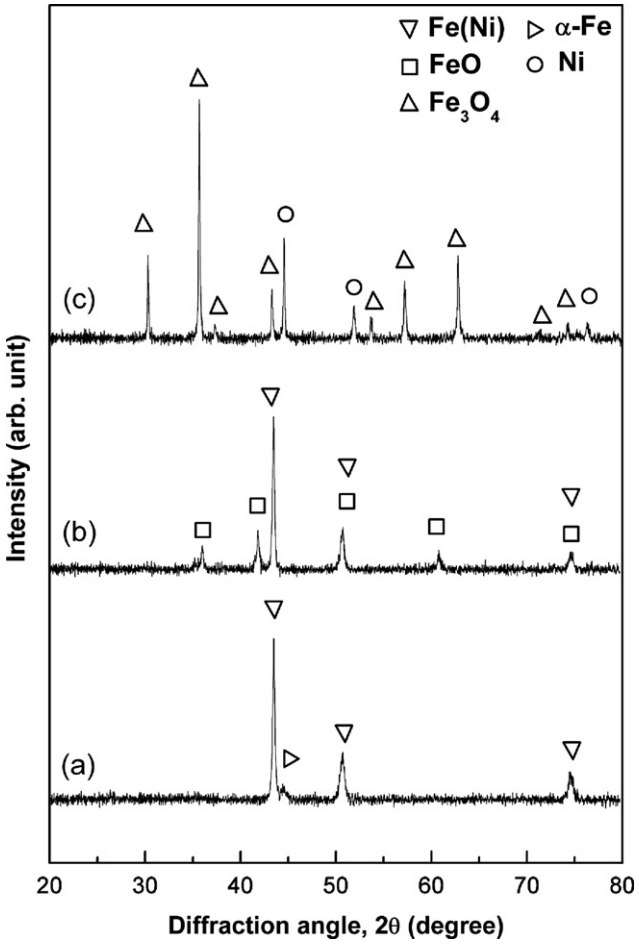

Fig. 6. X-ray diffraction images: (a) reduced Ni-ferrite, and reduced Ni–ferrite after water-splitting for production of H_2 at different time (b) 5 min and (c) 30 min.

The TGA curve of $NiFe_2O_4$ with CH_4 gas at 900 °C (single reduction process) demonstrated an ultimate weight loss of 25.66%, which means that approximately 3.8 oxygen atoms of the $NiFe_2O_4$ reacted with CH_4 gas and a nearly complete reduction was achieved. As a result, a major phase of Fe(Ni) alloys with a small amount of α-Fe in reduced Ni–ferrites was observed by XRD, as shown in Fig. 6(a). According to the equilibrium phase diagrams for Metal–Metal Oxide system redox reactions in the syngas redox (SGR) process for the reaction of CO_2/CO with H_2O/H_2, reduced iron oxide or iron metals are capable of decomposing steam (H_2O) for the generation of H_2 [5,11]. To test for the decomposition of H_2O into H_2 (water-splitting), steam (10 vol%) was introduced into the reactor with N_2 gas (60 sc/cm) at 900 °C. Fig. 7(a) shows the evolution flow rate of H_2 gases from the H_2O decomposition using reduced Ni–ferrites, reduced iron oxide, and reduced nickel oxide. Within 5 min of beginning the water-splitting tests, a maximum hydrogen flow rate of 19.4 mL/min was obtained for reduced iron oxide. By integrating the evolution flow rate of H_2 gas in Fig. 7(b), we obtained an H_2 evolution volume profile of approximately 250 ml over one hour. However, reduced Ni–ferrites demonstrated a strong ability to decompose steam (H_2O) into H_2, achieving a hydrogen flow rate of 16.6 mL/min within 5 min. (Fig. 7(a)). In addition, an H_2 evolution volume profile of approximately 30 ml was obtained within 5 min due to the phase transformation of α-Fe into FeO (Fig. 6(b)). After 30 min, the accumulated volume of H_2 remained at a constant value of 150 ml (Fig. 7(b)), indicating that the reduced Ni–ferrites had completely oxidized with steam to form a mixture phase of Fe_3O_4 and metallic nickel (Fig. 6(c)). Conversely, reduced nickel oxides or nickel metals are intrinsically less capable of water-splitting, which is consistent with the equilibrium phase diagrams of the SGR process [5,11].

For the practical application of oxide materials as oxygen carriers for CLP, ensuring the redox feasibility of the reoxidation process of the powder after the reduction process and steam decomposition is imperative. Fig. 8 shows the XRD patterns of the reoxidization of the oxidized sample with a mixture phase of Fe_3O_4 and nickel metals under air atmosphere at various temperatures. Interestingly, $NiFe_2O_4$ can be regenerated by reoxidization in air at 900 °C (Fig. 8(c)), whereupon catalytic activity is believed to be restored to its original value. Therefore, the redox cycling of $NiFe_2O_4$ was evaluated by thermogravimetric (TGA)

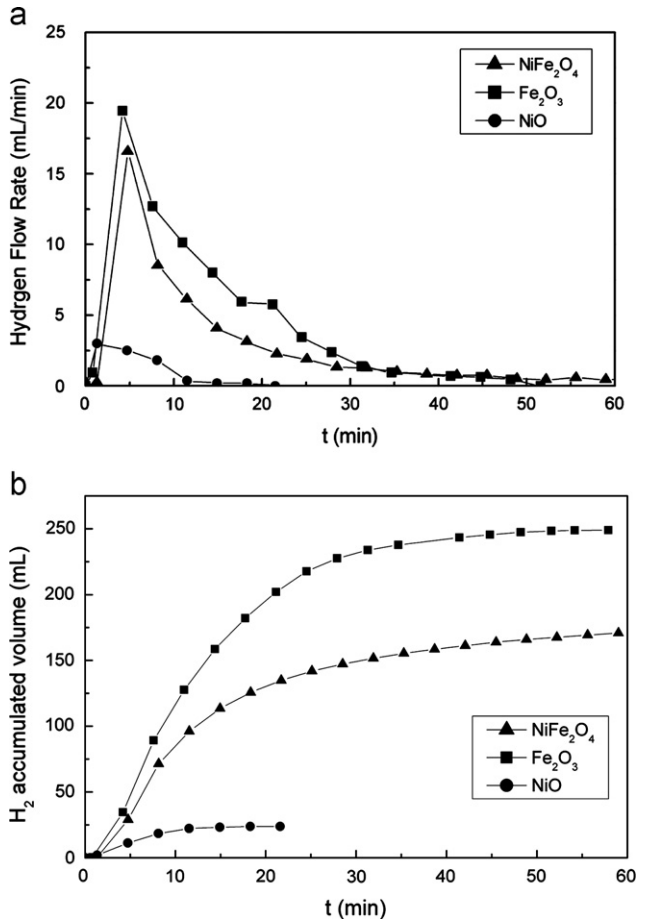

Fig. 7. H_2 evolution profile during the H_2O decomposition with various oxygen carriers at 900 °C: (a) hydrogen flow rate, and (b) accumulated volume of H_2.

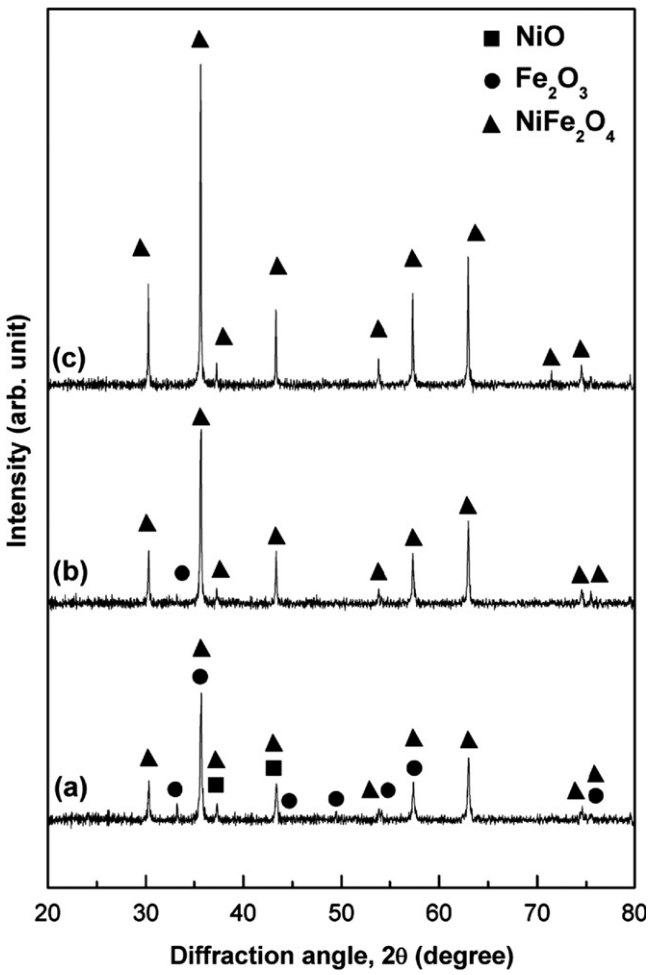

Fig. 8. X-ray diffraction of re-oxidation at different temperatures for reduced $NiFe_2O_4$ following production of H_2: (a) 700 °C, (b) 800 °C, and (c) 900 °C.

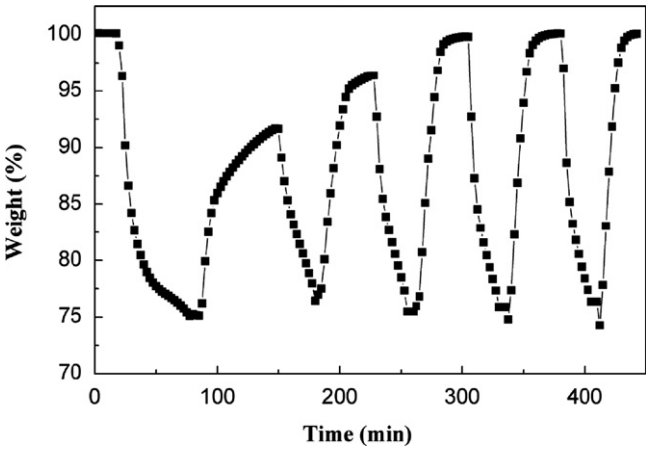

Fig. 9. Redox cycling performance of prepared $NiFe_2O_4$ oxygen carriers.

measurement under CH_4 gas and O_2/air atmospheres, respectively. After repeating the two-step process through five successive redox cycles at 900 °C (Fig. 9), the prepared $NiFe_2O_4$ powder demonstrated higher redox cycling behavior with no apparent degradation.

Kodama et al. proposed a two-step redox cycling process via solar methane reformation using a Ni-ferrite redox system, in which solar heat converted chemical fuels to produce co-rich syngas and hydrogen in separate steps [20]. They also pointed out that using Ni–ferrite as the oxidant toward methane (CH_4) under solar-simulated irradiation of high flux visible light yielded more than 90% methane conversion with feasible reversibility following oxidization above 800 °C. This study also proposed a three steps mechanism for redox cycling using $NiFe_2O_4$ powder in a chemical looping process with methane.

In the first process, the prepared $NiFe_2O_4$ powder was fully reduced to metals (Fe(Ni) alloys and α-Fe) through a reaction with methane to yield gaseous CO_2 and H_2O. Subsequently, Fe (Ni) alloys and α-Fe encountered steam to generate H_2 gas and form the mixture phase of Fe_3O_4 and Ni. Finally, the mixture phase of Fe_3O_4 and Ni was reoxidized back to the original ferrite phase at 900 °C. These results demonstrate the applicability of using $NiFe_2O_4$ in a high temperature solid state reaction as an oxygen carrier for a chemical looping process.

Reduction:

$$NiFe_2O_{4(s)} + CH_{4(g)} \xrightarrow{\Delta} Fe(Ni)_{(s)} + \alpha\text{-}Fe_{(s)} + CO_{2(g)} + H_2O_{(g)} \quad (4)$$

Water decomposition:

$$\mathrm{Fe(Ni)}_{(s)} + \alpha\text{-}\mathrm{Fe}_{(s)} + \mathrm{H_2O}_{(g)} \xrightarrow{\Delta} \mathrm{Fe_3O_{4(s)}} + \mathrm{Ni}_{(s)} + \mathrm{H}_{2(g)} \quad (5)$$

Reoxidization:

$$\mathrm{Ni}_{(s)} + \mathrm{Fe_3O_{4(s)}} + \mathrm{O}_{2(g)}(\text{from air}) \xrightarrow{\Delta} \mathrm{NiO}_{(s)} + \mathrm{Fe_2O_{3(s)}} \xrightarrow{\Delta} \mathrm{NiFe_2O_{4(s)}}_{4(s)}{}^{2} \quad (6)$$

4. Conclusions

Nickel ferrite ($NiFe_2O_4$) with a spinel single phase was prepared through ball milling of equimolar NiO and Fe_2O_3 and a high temperature solid state reaction. Only one stepwise reduction process was observed in the preparation of $NiFe_2O_4$ by TGA under CH_4 atmosphere, indicating that the addition of NiO to Fe_2O_3 could be used to recover the lower reduction kinetics of iron oxide. Following the first step of complete reduction, the reduced nickel ferrite comprised Fe(Ni) alloy and α-Fe was capable of promoting the production of hydrogen by water-splitting with a yield of 150 mL within 30 min, which is superior to that of nickel. After repeating the two-step process through five successive redox cycles at 900 °C, the reversibility of the process was demonstrated with no apparent degradation. This supports the feasibility of the proposed mechanism of redox cycling using $NiFe_2O_4$ as an oxygen carrier for a chemical looping process (CLP), with performance exceeding that of iron oxide.

Acknowledgments

The authors would like to thank the National Science Council of the Republic of China for financially supporting this research under contract no. NSC-98-2221-E-011-150 and NSC-100-3113-E-007-005.

References

[1] S. Arrhenius, On the influence of carbonic acid in the air upon the temperature of the ground, Philosophical Magazine 41 (1896) 237.
[2] M. Ishida, H. Jin, A novel combustor based on chemical-looping reactions and its reaction kinetics, Journal of Chemical Engineering of Japan 27 (1994) 296–301.
[3] L.F. de Diego, F. García-Labiano, J. Adánez, P. Gayán, A. Abad, B.M. Corbella, J.M. Palacios, Development of Cu-based oxygen carriers for chemical-looping combustion, Fuel 83 (2004) 1749–1757.
[4] F. García-Labiano, J. Adánez, L.F. de Diego, P. Gayán, A. Abad, Effect of pressure on the behavior of copper-, iron-, and nickel-based oxygen carriers for chemical-looping combustion, Energy Fuels 20 (2006) 26–33.
[5] P. Gupta, L.G. Velazquez-Vargas, L.S. Fan, Syngas redox (SGR) process to produce hydrogen from coal derived syngas, Energy Fuels 21 (2007) 2900–2908.
[6] W.K. Lewis, E.R. Gilliland, Production of Pure Carbon Dioxide, US Patent no. 2665972, 1954.
[7] R. Siriwardane, H. Tian, D. Miller, G. Richards, T. Simonyi, J. Poston, Evaluation of reaction mechanism of coal-metal oxide interactions in chemical-looping combustion, Combust. Flame 157 (2010) 2198–2208.
[8] K. Svoboda, G. Slowinski, J. Rogut, D. Baxter, Thermodynamic possibilities and constraints for pure hydrogen production by iron based chemical looping process at lower temperatures, Energy Conversion and Management 48 (2007) 3063–3073.
[9] K. Svoboda, A. Siewiorek, D. Baxter, J. Rogut, M. Pohořelỳ, Thermodynamic possibilities and constraints for pure hydrogen production by a nickel and cobalt-based chemical looping process at lower temperatures, Energy Conversion and Management 49 (2008) 221–231.
[10] K. Svoboda, A. Siewiorek, D. Baxter, J. Rogut, M. Pohořelỳ, Thermodynamic possibilities and constraints of pure hydrogen production by a chromium, nickel, and manganese-based chemical looping process at lower temperatures, Chemical Papers 61 (2007) 110–120.
[11] F. Li, H.R. Kim, D. Sridhar, F. Wang, L. Zeng, J. Chen, L.S. Fan, Syngas chemical looping gasification process: oxygen carrier particle selection and performance, Energy Fuels 23 (2009) 4182–4189.
[12] J. Bessières, A. Bessières, J.J. Heizmann, Iron oxide reduction kinetics by hydrogen, International Journal of Hydrogen Energy 5 (1980) 585–595.
[13] H.Y. Lin, Y.W. Chen, C. Li, The mechanism of reduction of iron oxide by hydrogen, Thermochimica Acta 400 (2003) 61–67.
[14] M. Shimokawabe, R. Furuichi, T. Ishii, Influence of the preparation history of $\alpha\text{-}Fe_20_3$ on its reactivity for hydrogen reduction, Thermochimica Acta 28 (1979) 287–305.
[15] P. Erri, A. Varma, Solution combustion synthesized oxygen carriers for chemical looping combustion, Chemical Engineering Science 62 (2007) 5682–5687.
[16] K. Otsuka, A. Mito, S. Takenaka, I. Yamanaka, Production of hydrogen from methane without CO_2-emission mediated by indium oxide and iron oxide, International Journal of Hydrogen Energy 26 (2001) 191–194.
[17] S. Takenaka, V.D.T. Son, K. Otsuka, Storage and supply of pure hydrogen from methane mediated by modified iron oxides, Energy Fuels 18 (2004) 820–829.
[18] G. Azimi, H. Leion, T. Mattisson, A. Lyngfelt, Chemical-looping with oxygen uncoupling using combined Mn-Fe oxides, testing in batch fluidized bed, Energy Procedia 4 (2011) 370–377.
[19] J.A. Peña, E. Lorente, E. Romero, J. Herguido, Kinetic study of the redox process for storing hydrogen: reduction stage, Catalysis Today 116 (2006) 439–444.
[20] T. Kodama, T. Shimizu, T. Satoh, M. Nakata, K.I. Shimizu, Stepwise production of co-rich syngas and hydrogen via solar methane reforming by using a Ni(II)–ferrite redox system, Solar Energy 73 (2002) 363–374.
[21] A. Pineau, N. Kanari, I. Gaballah, Kinetics of reduction of iron oxides by H_2 part I: low temperature reduction of hematite, Thermochimica Acta 447 (2006) 89–100.
[22] M.H. Khedr, Isothermal reduction kinetics at 900–1100 °C of $NiFe_2O_4$ sintered at 1000–1200 °C, Journal of Analytical and Applied Pyrolysis 73 (2005) 123–129.
[23] M.H. Khedr, Isothermal reduction kinetics of Fe_2O_3 Mixed with 1–10% Cr_2O_3 at 1173–1473 K, ISIJ International 40 (2000) 309–314.